


Optimized excitonic transport mediated by local energy defects: Survival of optimization laws in the presence of dephasing

Lucie Pepe,¹ Vincent Pouthier,² and Saad Yalouz ^{1,*}

¹Laboratoire de Chimie Quantique, Institut de Chimie, CNRS/Université de Strasbourg, 67000 Strasbourg, France

²Institut UTINAM, Université de Franche-Comté, CNRS UMR 6213, 25030 Besançon, France



(Received 29 August 2023; accepted 7 December 2023; published 8 January 2024)

In an extended star with peripheral defects and a core occupied by a trap, it has been shown that exciton-mediated energy transport from the periphery to the core can be optimized [S. Yalouz *et al.*, *Phys. Rev. E* **106**, 064313 (2022)]. If the defects are judiciously chosen, then the exciton dynamics is isomorphic to that of an asymmetric chain and a speedup of the excitonic propagation is observed. Here we extend this previous work by considering that the exciton in both an extended star and an asymmetric chain is perturbed by the presence of a dephasing environment. Simulating the dynamics using a Lindblad master equation, two questions are addressed: How does the environment affect the energy transport on these two networks? and Do the two systems still behave equivalently in the presence of dephasing? Our results reveal that the timescale for the exciton dynamics strongly depends on the nature of the network. But quite surprisingly, the two networks behave similarly regarding the survival of their optimization law. In both cases, the energy transport can be improved using the same original optimal tuning of energy defects as long as the dephasing remains weak. However, for moderate or strong dephasing, the optimization law is lost due to quantum Zeno effect.

DOI: [10.1103/PhysRevE.109.014303](https://doi.org/10.1103/PhysRevE.109.014303)

I. INTRODUCTION

Studying exciton-mediated energy transport in molecular lattices has a long history that can be traced back to the 1960s–1970s [1–4]. At that time, and during the following decades, the research was realized to understand the behavior of translationally invariant molecular crystals, with particular emphasis on the characterization of their optical properties [5]. Different features were considered, i.e., the study of the exciton-phonon interaction to explain relaxation processes, optical line shapes, and quantum diffusion [6–11], the influence of defects to characterize specific optical response and to investigate localization phenomena [12–15], and the analysis of nonlinear effects to describe both the nonlinear excitonic optical response [16] and the formation of nonlinear objects such as solitons [17].

Nowadays, with the development of quantum technologies, new ideas have emerged, and it has been pointed out that exploiting exciton propagation in complex networks could be used to carry either quantum information, or energy, at nanoscale [18]. Indeed, on complex networks, the delocalization of an exciton defines a physical realization of a continuous time quantum walk (CTQW) [19]. Widely studied in recent years, the concept of CTQW has been used to answer a variety of questions in quantum information theory ranging from the realization of perfect quantum state transfer [20] to the development of high-performance algorithms [21–23]. On another note, this paradigm has been also widely used to study the energy transfer on complex networks with a

specific focus on the role of the topology [24,25], the effect of disorder [18,26], and the presence of traps [27,28] to cite but a few. In the present paper, we are interested in this second aspect where complex networks architectures are considered as a medium for efficient exciton-mediated energy transport at the nanoscale. Such an idea was first pointed out by Mukamel [29] who suggested that excitons could be exploited in dendrimers to design artificial light-harvesting complexes (LHC) [30–41]. A dendrimer is a chemical treelike structure formed by several dendritic branches that emanate out from a central core [42–44]. Therefore, the functionalization of the terminal groups by chromophores favors light harvesting. The absorbed light generates local photoexcitations, i.e., Frenkel excitons, that propagate along the branches and converge towards the central core which contains either a fluorescent trap, a reaction center, or a chemical sensor [45,46].

Inspired by these treelike architectures, the excitonic CTQW on an extended star was studied recently to highlight the realization of an efficient photoexcitation transfer [47]. In this context, it was considered that the periphery of the star was functionalized by tunable energy defects, while the core was occupied by a trap. The absorption of light by the defects generates an exciton in an initial state uniformly delocalized over the peripheral sites. The energy is then transferred via an excitonic CTQW from the periphery to the core where an irreversible absorption process occurs due to the presence of the trap. The investigations realized on this prototype LHC allowed to evidence the possibility to strongly optimize the resulting energy transfer–absorption process. Depending on both the number and the length of the branches, it has been shown that if the energy defects are judiciously chosen, then the initial state localized at the periphery may hybridize with

*yalouzsad@gmail.com

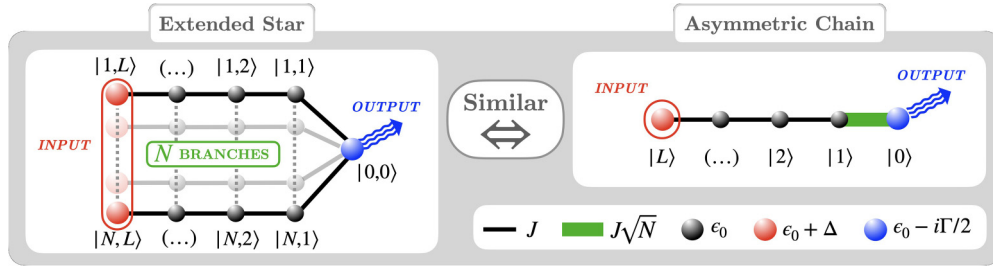


FIG. 1. Illustration of the two networks considered in our study. Left: The extended star which is formed by a central core acting as a trap with an absorbing rate Γ (blue output site on the right), connected to N branches containing L sites. Each branches carries on its extremity an energy defect with a tunable amplitude Δ (red-circled input sites on the left). The exciton can hop between each connected site *via* a hopping constant J . Right: The asymmetric chain which carries on its left extremity an energy defect with a tunable amplitude Δ (single red-circled input site) and on the other side a trap with absorbing rate Γ (blue output site on the right). The exciton can hop between each connected site *via* a hopping constant J , except between the two rightmost sites where it is $J\sqrt{N}$.

a state localized on the core (for a detailed demonstration, see discussion section in Ref. [47]). Consequently, a speedup of the excitonic propagation was observed revealing the potential of the extended star as a prototype artificial LHC.

Interestingly, in Ref. [47] it was also highlighted that the optimal excitonic transfer occurring on the extended star was actually isomorphic to that of an asymmetric chain (when the exciton is initially delocalized over the periphery of the star). This chain, whose length is equal to that of the branches of the star, involves sites whose meaning can be understood as follows. The first site refers to the trap, the second site refers to an exciton delocalized over the first site of the branches of the star, the third site refers to an exciton delocalized over the second site of the branches of the star, and so on. The resulting isomorphism between the two networks reveals a fundamental point: both the extended star and the asymmetric chain act as equivalent LHC prototypes that can be designed to produce the same optimal energy transfer and absorption. At this step, it should be noted here that all these results were obtained assuming that the two quantum systems were closed. Naturally, we can wonder now about the evolution of the optimal transport in both systems when a more realistic description is considered, including for example the presence of an external environment.

Indeed, in nature, excitons no longer propagate freely: They behave as open quantum systems interacting with the remaining degrees of freedom of the medium, usually associated with a phonon bath [3]. The phonons are thus responsible for quantum dephasing [48–50] that drastically modifies the way excitons delocalize. Generally acting as a disruptive ingredient, the presence of a phonon bath tends to prevent the conservation of superposed states. It thus generates a transition between an efficient coherent propagation and an inefficient incoherent diffusive motion [51,52].

Motivated by this view, in the present paper we want to address two questions: How would the presence of the environment affect the energy transport on both the extended star and the asymmetric chain? and Do the two networks still behave equivalently in the presence of dephasing? To this end, the excitonic dynamics on both networks will be revisited in this work by considering the influence of an external dephasing environment. To proceed, a standard stochastic approach is used by assuming that the environment behaves as

a Gaussian Markovian δ -correlated stochastic potential field acting on the exciton [53–57]. Within this model, a generalized master equation (GME) is established for describing the time evolution of the exciton reduced density matrix (RDM). The knowledge of the RDM allows us to compute in principle all the observables needed to characterize the exciton dynamics.

The paper is organized as follows, in Sec. II the extended star and the asymmetric chain are introduced and the exciton Hamiltonians are defined. Then the relevant observables required for characterizing the dynamics and the absorption process are described. In Sec. III, a numerical analysis is performed to characterize the absorption process. Finally, in Sec. IV the results are discussed and interpreted using analytical approaches.

II. THEORETICAL BACKGROUND

A. Model Hamiltonians

The two networks we consider are the extended star and the asymmetric chain, as illustrated in Fig. 1. In the absence of the environment, both networks exhibit the same excitonic dynamics provided that the exciton starts from the sites carrying the energy defects. More precisely, an exciton uniformly distributed over the input sites on the extended star (red-circled sites in Fig. 1) exhibits a time evolution that is isomorphic to that of a single exciton starting from the input site of the asymmetric chain (single red-circled site). This similarity has been highlighted in our previous work (see Ref. [47]) and will be discussed and illustrated again in the present work (later on in Sec. III A). In both networks, the resulting dynamics is entirely ruled by a common set of parameters that define the tight-binding Hamiltonians of each system. In the following, we will introduce the form of these Hamiltonians and explain the signification of all the associated parameters.

1. Extended star graph

The excitonic dynamics on the extended star network is described by a standard tight-binding model [3] that closely follows the graph's architecture (see Fig. 1). Within this model, we assume that each site of the network is occupied by a molecular subunit whose internal dynamics is described by

a two-level system. Let $|b, s\rangle$ stand for the state in which the (b, s) th two-level system (i.e., site) occupies its first excited state, the other two-level systems remaining in their ground state. Here (b, s) denotes the s th site ($s = 1, \dots, L$) of the b th branch ($b = 1, \dots, N$) of the star. The site $(b, s) = (0, 0)$ refers to the core of the star. Note that the star involves $\mathcal{N}_S = 1 + NL$ sites. Let ϵ_0 denote the excited state energy of the two-level systems except those of the periphery and of the core of the graph. As illustrated in Fig. 1, the terminal groups are occupied by energy defects whose excitation energy is shifted by an amount Δ according to $\epsilon_0 + \Delta$. The core of the graph is occupied by a trap that is responsible for the irreversible decay (i.e., absorption) of the exciton. It is characterized by a complex self-energy $\epsilon_0 - i\Gamma/2$, where Γ defines the exciton decay rate [58,59]. Finally, the exciton can jump between connected nodes *via* a hopping constant J .

Following these notations, the Hamiltonian governing the exciton dynamics on the extended star is defined as (the convention $\hbar = 1$ is used throughout the paper)

$$H = \left(\epsilon_0 - i\frac{\Gamma}{2} \right) |00\rangle\langle 00| + \sum_{b=1}^N \sum_{s=1}^L (\epsilon_0 + \Delta\delta_{sL}) |b, s\rangle\langle b, s| + \sum_{b=1}^N J(|00\rangle\langle b, 1| + |b, 1\rangle\langle 00|) + \sum_{b=1}^N \sum_{s=1}^{L-1} J(|b, s\rangle\langle b, s+1| + |b, s+1\rangle\langle b, s|), \quad (1)$$

where δ is the Kronecker symbol.

2. Asymmetric chain

Following the same philosophy, the exciton dynamics on the asymmetric chain (right part of Fig. 1) is described according to a tight-binding model,

$$H = \sum_{s=0}^L \left(\epsilon_0 + \Delta\delta_{sL} - i\frac{\Gamma}{2}\delta_{s0} \right) |s\rangle\langle s| + \sum_{s=1}^{L-1} J(|s\rangle\langle s+1| + |s+1\rangle\langle s|) + J\sqrt{N}(|1\rangle\langle 0| + |0\rangle\langle 1|). \quad (2)$$

Here the state $|s\rangle$ describes the situation where the exciton occupies the s th site of the chain. All sites have a local excitation energy ϵ_0 except the two extremities of the chain: The site $s = L$ carries an energy defect $\epsilon_0 + \Delta$, and the site $s = 0$ acts as a trap with a complex energy $\epsilon_0 - i\Gamma/2$. All sites are connected to their nearest neighbors with a hopping constant J , except the couple of sites $s = 0$ and 1 connected by an amplitude $J\sqrt{N}$. The presence of the parameter N originates in the equivalence between the dynamics of the asymmetric chain and that of the extended star, as established in details in Appendix A. Note that the total number of sites is $\mathcal{N}_S = 1 + L$.

B. Open quantum system dynamics

To describe the open quantum dynamics of the exciton, we consider a pure dephasing phononic environment modeled by the so-called Haken-Strobl-Reineker master equation [2,53,54]. In this model, the time evolution of the excitonic RDM $\rho(t)$ is governed by the GME,

$$\partial_t \rho_{xy} = -i \sum_z (H_{xz} \rho_{zy} - \rho_{xz} H_{zy}^\dagger) - \gamma(1 - \delta_{xy}) \rho_{xy}, \quad (3)$$

which is expressed in the local site basis with generic indices x, y and z (a local state $|x\rangle$ refers either to a state $|b, s\rangle$ for the star graph or to a state $|s\rangle$ for the chain). Here H represents the non-Hermitian network Hamiltonian, and γ is the dephasing rate responsible for the irreversible decay of the quantum coherence $\rho_{xy} = \langle x|\rho|y\rangle$ between two distinct sites with generic indices x and y . In the scope of this work, the master equation represented by Eq. (3) accounts solely for the dephasing environment. Nevertheless, practical scenarios may encompass additional relaxation sources, such as excitonic finite lifetime attributed to phenomena like optical recombination. While these elements have been explored in various prior studies (see, for example, Refs. [60,61]), we have opted for simplicity in our model for this study, thereby excluding such effects.

To simulate the open quantum dynamics of the exciton, one employs the so-called Fock-Liouville space (FLS) method [16] which consists in a vectorization of the master equation [see Eq. (3)]. In this approach, the density matrix ρ is encoded into a single vector noted $|\rho\rangle\rangle$ (i.e., $|\rho\rangle$ is a flattened version of the RDM ρ). This allows us to rewrite the GME under the form of a generic set of linear differential equations. The constant coefficients of this set (associated to the Hamiltonian matrix elements and the dephasing rate) are gathered into the so-called Liouvillian matrix \mathcal{L} , and the GME reads then

$$\partial_t |\rho(t)\rangle\rangle = \mathcal{L} |\rho(t)\rangle\rangle. \quad (4)$$

The formal exponential solution of this equation gives access to the time evolution of the RDM at time t such that

$$|\rho(t)\rangle\rangle = \exp(\mathcal{L}t) |\rho(0)\rangle\rangle, \quad (5)$$

where $\exp(\mathcal{L}t)$ is the time-evolution superoperator

$$\exp(\mathcal{L}t) = \sum_k^{\mathcal{N}_S^2} \exp(\Lambda_k t) \frac{|\Lambda_k^R\rangle\rangle\langle\langle \Lambda_k^L|}{\langle\langle \Lambda_k^L | \Lambda_k^R \rangle\rangle}, \quad (6)$$

where $|\Lambda_k^L\rangle\rangle$ and $|\Lambda_k^R\rangle\rangle$ are the left and right eigenvectors of the Liouvillian matrix \mathcal{L} and Λ_k their associated complex eigenvalue. Note that the numerical cost of the FLS method scales in \mathcal{N}_S^6 which can be problematic when addressing large systems such as the star network. Fortunately, for this network this can be alleviated by using the symmetries of the problem (see Appendix B).

From the knowledge of the time-evolution superoperator, different time-dependent observables may be evaluated. In this work, we will mainly focus on the absorption probability $P_A(t)$ expressed as

$$P_A(t) = 1 - \text{Tr}\{\rho(t)\}. \quad (7)$$

The measure $P_A(t)$ describes the probability for the exciton to be absorbed by the trap at time t . To characterize the absorption process on both networks, we also introduce the absorption time τ defined as

$$\tau \longrightarrow P_A(\tau) = 50\%, \quad (8)$$

which gives the characteristic time when half of the excitonic population is absorbed by the trap. In practice, the absorption time τ is determined *via* a numerical minimization (over the parameter t) of the cost function $\mathcal{C}(t) = [0.5 - P_A(t)]^2$ using the *Nelder-Mead* method from the *scipy* package [62].

III. NUMERICAL RESULTS

In this section, the previous formalism is applied to study the absorption process on both the extended star graph and the asymmetric chain. In a first part, we will recall the main features observed without dephasing (i.e., $\gamma = 0$). In a second part, we will include the environment (i.e., $\gamma > 0$) and illustrate the changes that occur in the absorption process. Note that in all our simulations, the initial conditions of the dynamics are always the same: a uniform excitonic delocalization on the star's peripheral defects and an excitonic localization on the single defect of the asymmetric chain (see Fig. 1). The hopping constant J is used as the energy reference (i.e., $J = 1$), the absorption rate is fixed to $\Gamma = 0.1J$, and we consider $N > 2$.

A. Absorption without dephasing ($\gamma = 0$): Optimal energy defects tuning

When $\gamma = 0$, both the extended star and the asymmetric chain behave in the same way. In this case, we have shown previously the existence of an optimal value of the energy defect amplitude that is [47]

$$\Delta^{\text{opt}} \approx \sqrt{N-1}J. \quad (9)$$

Around this value, the absorption process presents a strong speedup, namely a reduction of the absorption time τ , provided that the length L is sufficiently short. To illustrate this feature, we show in Fig. 2(a) the Δ dependence of the absorption time τ for $N = 5$ and for $L = 4, 6, 8$, and 10 . As readily seen here, a local minimum of the absorption time systematically appears around the critical value $\Delta^{\text{opt}} \approx \sqrt{N-1}J$, whatever L . In some cases, this local minimum can go even below the absorption time obtained in the absence of defects (i.e., when $\Delta = 0$). This is the case for example with $L \leq 6$ where the absorption time τ reaches a global minimum when $\Delta \rightarrow \Delta^{\text{opt}}$ [see black curve with circles and brown curve with triangle in Fig. 2(a)]. However, this is no longer the case for larger L values like $L = 8$ or 10 (see red curve with crosses and orange curve with diamonds).

These results highlight the existence of a “speedup” for the absorption process which depends on both N and L . To better evidence this feature, we introduce a measure \mathcal{S} of the absorption speedup, which is

$$\mathcal{S} = 1 - \frac{\tau(\Delta^{\text{opt}})}{\tau(\Delta = 0)}. \quad (10)$$

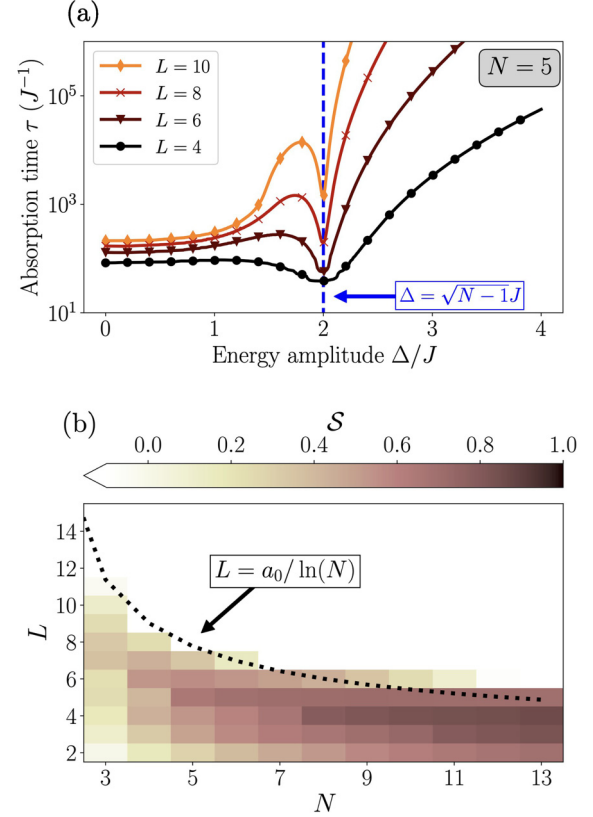


FIG. 2. Evidence of an excitonic absorption speedup by energy defect tuning (with $\gamma = 0$). (a) Evolution of τ as a function of Δ for $N = 5$ and $L = 4$ (black curve with circles), $L = 6$ (brown curve with triangles), $L = 8$ (red curve with crosses), and $L = 10$ (orange curve with diamonds). The particular value $\Delta = \sqrt{N-1}J$ where a strong acceleration of the absorption process occurs is marked by a dashed blue vertical line. (b) Speedup \mathcal{S} [Eq. (10)] of the absorption process in the (N, L) -parameter space. Dark colors show where a speedup occurs (i.e., $\mathcal{S} > 0$), whereas white areas reveal where there is none (i.e., $\mathcal{S} \leq 0$). The dotted black curve describes the logarithmic limit [see Eq. (11)] defining the region where a speedup is produced.

With this measure, we evaluate the reduction (or increase) in the absorption time obtained in the presence of energy defects tuned as $\Delta = \Delta^{\text{opt}}$ compared to the case where no defect is considered (i.e., when $\Delta = 0$). By definition, $\mathcal{S} \in]-\infty, 1]$ so that the closer \mathcal{S} gets to 1, the more important is the speedup. Conversely, $\mathcal{S} < 0$ indicates that no speedup is produced at all. In the latter case, the absorption time τ at $\Delta = \Delta^{\text{opt}}$ is just a local minimum in the Δ space but not a global one.

Figure 2(b) shows a heatmap of \mathcal{S} in the (L, N) -parameter space. In this figure, we deliberately choose to rescale the colormap to only highlight regions where a reduction is produced (i.e., where $\mathcal{S} > 0$) using a dark color gradient. White regions refer to situations in which no reduction in absorption time is produced (when $\Delta = \Delta^{\text{opt}}$). The present results clearly evidence a region in the (L, N) -parameter space where a strong speedup $\mathcal{S} > 0$ is produced. This region can be delimited by the following rule for the structural parameter L and N :

$$\mathcal{S} > 0 \implies L \leq L^*, \text{ with } L^* \approx \frac{a_0}{\ln(N)}, \quad (11)$$

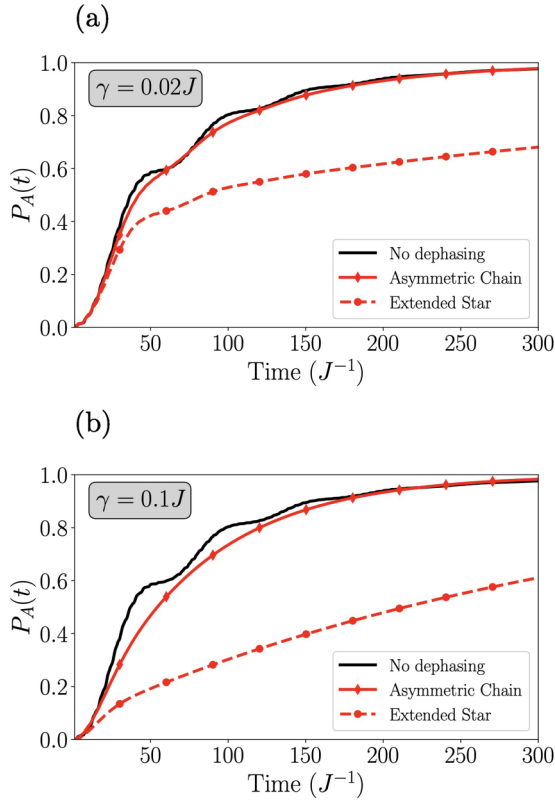


FIG. 3. Time evolution of the absorption probability $P_A(t)$ in both networks with dephasing $\gamma > 0$ ($N = L = 5$ and $\Delta^{\text{opt}} = \sqrt{N - 1}J$). (a) Weak dephasing $\gamma = 0.02J$. (b) Moderate dephasing $\gamma = 0.1J$. Full red lines (with diamonds) show the results for the asymmetric chain, while dashed curves (with circles) are for the extended star. Full black lines show the reference result when no dephasing is considered and both networks admit the same absorption process.

where $a_0 = 12.5$ is a numerical coefficient. For both networks we see here that the architectural parameter L is the main limiting factor for the appearance of the absorption process speedup.

B. Absorption with dephasing ($\gamma > 0$)

In this second section, we include the presence of a dephasing environment ($\gamma > 0$) and we illustrate the changes involved in the absorption process.

1. Evidence of different timescales for the absorption processes on the two networks

Let us first highlight an important feature observed in all our simulations: In the presence of the dephasing, the timescale for the realization of the absorption process is very different between both networks. To illustrate this feature, we show in Fig. 3 the time evolution of the absorbed population $P_A(t)$ for both networks with weak [$\gamma = 0.02J$ in Fig. 3(a)] and moderate [$\gamma = 0.1J$ in Fig. 3(b)] dephasing. In this figure, dashed red lines with circles illustrate the results obtained for the extended star, while full red lines with diamonds are used for the asymmetric chain. As a reference, we also show with

full black curves $P_A(t)$ when $\gamma = 0$ (i.e., the case where both networks behave the same).

In Fig. 3(a), we see that the presence of even a very weak dephasing amplitude leads to a different time evolution of the absorption process, depending on the considered network. For the asymmetric chain, $P_A(t)$ is barely affected by the dephasing, and the resulting absorption time $45J^{-1}$ is still quite close to that obtained without dephasing $37J^{-1}$. Conversely, more significant changes occur in the case of the extended star. Here the absorption process is slowed down and the absorption time becomes $\tau \sim 75J^{-1}$, which is almost twice as long as in the case where no dephasing is considered. As shown in Fig. 3(b), this slowdown becomes even more important when the dephasing rate reaches $\gamma = 0.1J$. In this case, the absorption time on the extended star increases considerably to $\tau \sim 200J^{-1}$ (four times more than in the reference case without dephasing). Conversely, the asymmetric chain shows only a very moderate increase in absorption time, which becomes $50J^{-1}$ (still fairly close to the case without dephasing).

2. Evolution of the energy absorption optimization law in the Δ -parameter space

At this point, a fundamental question arises: Is the energy-defect tuning $\Delta = \sqrt{N - 1}J$ still optimal for energy absorption in the presence of the environment? To address this question, the Δ dependence of the absorption time in different dephasing regimes is shown in Fig. 4 for the extended star [Fig. 4(a)] and for the chain [Fig. 4(b)]. We consider $N = L = 5$ and a color gradient is used to illustrate the behaviors obtained for three increasing dephasing amplitudes $\gamma = 0.01J$, $0.1J$, and $0.5J$. As a reference, we also show here the absorption time obtained when $\gamma = 0$ with a black dashed curve.

By comparing the results obtained for both networks, we see that the two systems present similarities and differences. First, let us highlight the most important property shared by the two systems: the survival of the optimal energy defect amplitude $\Delta = \sqrt{N - 1}J$. Indeed, for both networks the Δ -dependent absorption time curves still exhibit a global minimum for this specific energy defect amplitude, as long as the dephasing amplitude is $\gamma \leq 0.1J$ (i.e., weak regime). Beyond this value (moderate and strong dephasing regimes), the minimum disappears and no optimization is produced. Second, we can see from Fig. 4 that increasing γ tends to converge the profile of the curves around different central values. In the strong dephasing limit, the absorption time becomes almost Δ independent. It converges towards $\sim 200J^{-1}$ for the extended star and $\sim 50J^{-1}$ for the asymmetric chain. Note that these two limit values compare well with the order of magnitude defined by the analytical ratio $\ln(2)\mathcal{N}_S/\Gamma$ (refer to Sec. IV for a comprehensive explanation of its derivation) which gives here $180J^{-1}$ for the extended star and $42J^{-1}$ for the chain. We will show in Sec. IV that this analytical ratio is a key quantity for interpreting the evolution of absorption time in the presence of dephasing. Finally, let us mention that after converging around different limit values, an increase of the dephasing amplitude like $\gamma \gg 0.5J$ (very strong regime) tends to generate an overall shift of the absorption time curves towards greater values for both networks (not shown here).

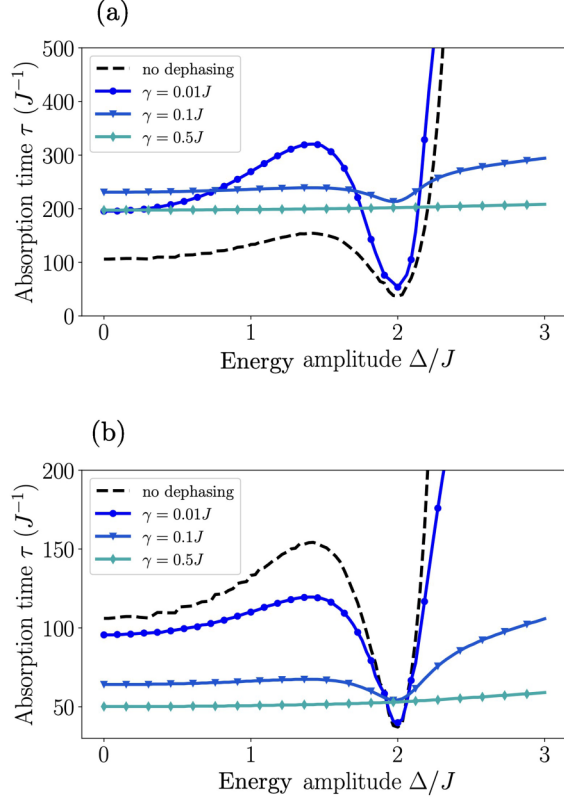


FIG. 4. Evolution of the absorption time τ with Δ for increasing values of dephasing rate $\gamma = 0.01J$ (dark blue curves with circles), $\gamma = 0.1J$ (blue curves with triangles), and $\gamma = 0.5J$ (cyan curves with diamonds) for $N = L = 5$. Dashed black lines show the reference result when no dephasing is considered. (a) Results for the extended star. (b) Results for the asymmetric chain.

Note that the Δ dependence of the absorption time τ is very general and is not limited to the case presented in Fig. 4. Indeed, many other numerical simulations (not shown here) have revealed that all the features presented here (i.e., survival of the optimization law, flattening of the curves, etc.) are recurrent features arising for both systems whatever the chosen architecture (N and L values), as long as this latter respects the architectural law $L < a_0/\ln(N)$ [given in Eq. (11)].

3. Assessing the survival of the excitonic absorption optimization law in the (L, N) -parameter space

All our results suggest that both networks present some similarities regarding the survival of the optimal setting of energy defects in the presence of dephasing. In this final part of our numerical study, we show that these similarities actually hold for different (L, N) configurations. To demonstrate this point, we introduce a γ -dependent measure of the absorption time speedup $\mathcal{S}(\gamma)$ that reads

$$\mathcal{S}(\gamma) = 1 - \frac{\tau(\gamma, \Delta^{\text{opt}})}{\tau(\gamma, \Delta = 0)}. \quad (12)$$

This measure is inspired by the one introduced in Eq. (10) (with $\gamma = 0$) with the difference that it now includes the effect of the dephasing on absorption time. We use this measure as an indicator for assessing the survival of the optimal tuning

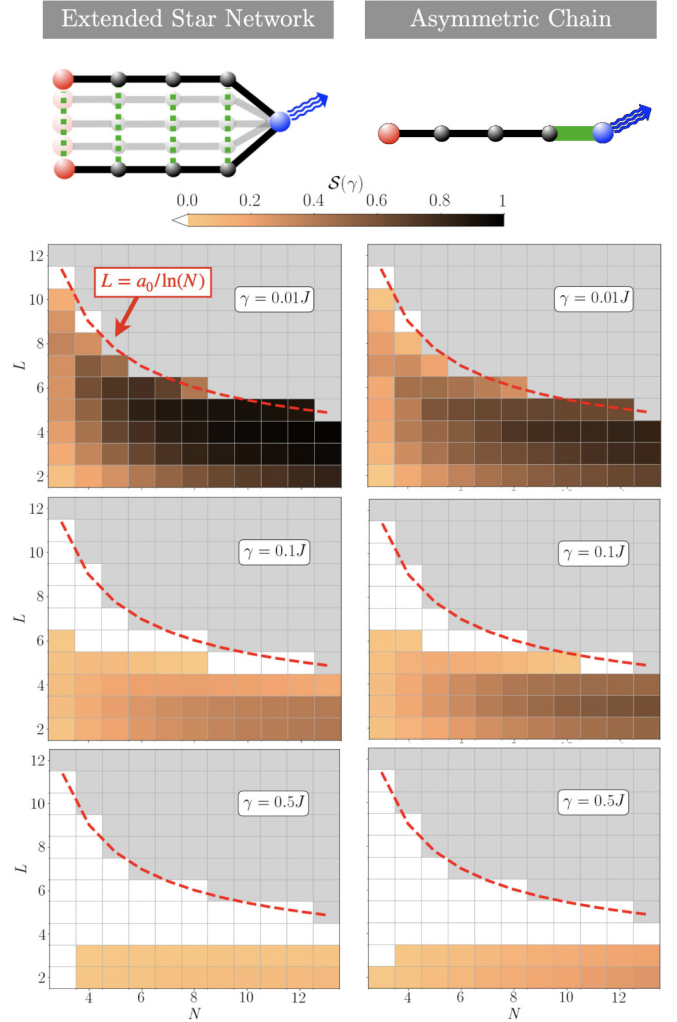


FIG. 5. Evolution of the dephasing-dependent measure $\mathcal{S}(\gamma)$ [as given in Eq. (12)] in the (L, N) -parameter space for both networks and increasing values of dephasing rate. Left and right columns respectively show the results for the extended star and the asymmetric chain. Top to bottom rows show results for $\gamma = 0.01J$, $0.1J$, and $0.5J$. A color gradient (ranging from orange to black) is used to show the regions where the absorption optimization mediated by the energy defects is still present [i.e., $\mathcal{S}(\gamma) > 0$]. White color is used wherever the optimization is lost $\mathcal{S}(\gamma) \leq 0$. Note that we only focus here on the region below the red dashed curves where the optimization was originally detected in the absence of dephasing (see Sec. III A). The rest of the space (on top of the red dashed curves) is thus represented with a uniform gray area.

$\Delta^{\text{opt}} = \sqrt{N-1}J$ of the energy defects. Here $\mathcal{S}(\gamma) > 0$ indicates a survival of the optimal tuning, i.e., the absorption time still presents a minimum when $\Delta = \Delta^{\text{opt}}$. Conversely, $\mathcal{S}(\gamma) \leq 0$ indicates that the minimum has been removed and no optimization can be produced. Note that $\mathcal{S}(\gamma)$ only evaluates the survival of the minimum for the absorption time, but it does not quantify the presence of a global offset as discussed in Sec. III B 2. In Fig. 5, we illustrate the evolution of $\mathcal{S}(\gamma)$ in the (L, N) -parameter space for increasing values of dephasing (from $\gamma = 0.01J$ to $0.5J$) with a series of heatmaps. Left and right columns respectively show the results obtained for the

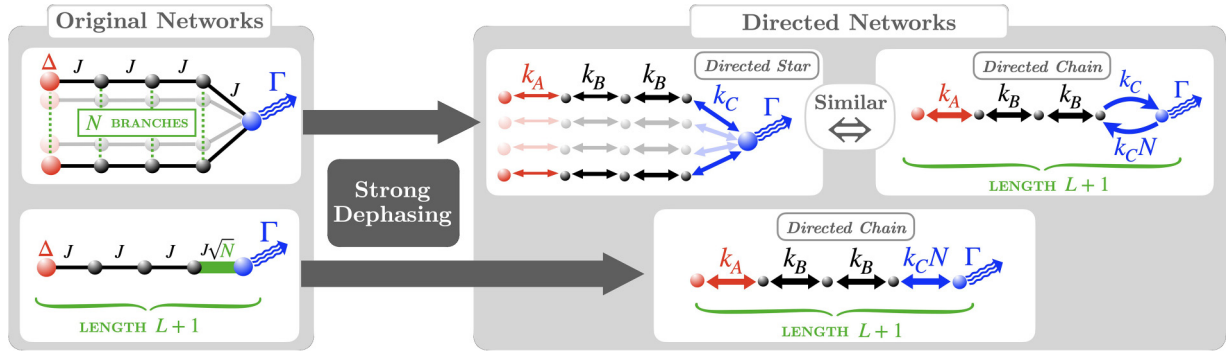


FIG. 6. Illustration of the change of behavior for the two networks considered in our study in the presence of strong dephasing. When γ is assumed to be large enough, both networks act as directed chains with rates k_A , k_B , k_C , and Γ . The two directed networks are very similar, except for the rates connecting the trap to its first neighbor (right part of the chains).

extended star network and the asymmetric chain. The rows from top to bottom show results for weak to moderate dephasing. Note that one focuses only on the (L, N) -parameter subspace where optimization was initially detected in the absence of dephasing [below the red dashed curves defined by Eq. (11)]. The rest of the (L, N) -parameter space (on top of the red dashed curves) is thus represented with a uniform gray area. The orange-black gradient shows regions where optimization is still present, while white areas show regions where it has been lost.

As readily seen in Fig. 5, both networks exhibit very similar behaviors for the evolution of $\mathcal{S}(\gamma)$ as γ increases. For weak dephasing $\gamma = 0.01J$ (see first row in Fig. 5), we observe a positive amplitude $\mathcal{S}(\gamma) > 0$ almost everywhere in the (L, N) -parameter space, which indicates the survival of the optimization for all the configurations. Then, when the value of dephasing increases to $\gamma \sim 0.1J$ (see second row in Fig. 5), one can see that this general property does not hold anymore. Around this value of dephasing, one begins to detect the arising of (L, N) configurations for which the measure becomes null or negative $\mathcal{S}(\gamma) \leq 0$, as indicated by the arising of large white areas below the red curve. When the dephasing reaches the moderate regime with $\gamma = 0.5J$, we observe an (almost) complete transition in the (L, N) -parameter space (third row in Fig. 5). In the latter case, the white zone extends over a large part of (L, N) configurations, revealing that the absorption optimization mediated by energy defects at $\Delta = \sqrt{N-1}J$ is lost on both networks. Note that additional simulations (not shown here) have shown that the absorption optimization completely disappears when one increases the dephasing to even larger values $\gamma \gg 0.5J$ (i.e., the white area spreads everywhere).

IV. INTERPRETATION OF THE ABSORPTION PROCESS

Our numerical study allowed to evidence a series of features. First, it has been shown that the presence of dephasing rescales the time evolution of the energy absorption process depending on the considered network. The process becomes globally much slower for the extended star than for the asymmetric chain. Second, one observed that both networks present very similar behaviors regarding the survival of the energy absorption optimization law. In both cases, a minimum of the absorption time τ still arises around the value of energy defect $\Delta^{\text{opt}} = \sqrt{N-1}J$, as long as the dephasing remains

weak enough. Finally, as γ increases to reach intermediate and strong dephasing regimes (typically $\gamma > 0.1J$), it has been shown that the optimization law no longer holds in both networks, whatever the (L, N) -configuration considered.

A. Excitonic diffusion view: From undirected to directed networks

To interpret our numerical results, we realize an analytical development based on the strong dephasing limit. In this context, the GME Eq. (3) can actually be replaced by a classical “rate equation” that reads

$$\partial_t \mathbf{P}(t) = \mathbf{K} \mathbf{P}(t). \quad (13)$$

This equation describes the time evolution of the excitonic populations ρ_{ss} on the sites of a network, which are collected into the vector \mathbf{P} of size \mathcal{N}_S (with $P_s = \rho_{ss}$). Here \mathbf{K} is the matrix whose elements encode the different rates governing the kinetic of the excitonic populations. As explained in Ref. [63], the determination of the excitonic rates in the strong dephasing limit is achieved following several steps. First, one starts from the GME expressed in the site basis [see Eq. (3)]. Then, assuming that the dephasing is strong enough, we consider stationary conditions for the quantum coherences ($\partial_t \rho_{xy} = 0$) between nearest neighbor sites, originally connected by a hopping constant (see Fig. 1). Every other “long-range” quantum coherences are neglected. Next, the short-range coherences ρ_{xy} are expressed in terms of the populations ρ_{xx} and ρ_{yy} . Using this redefinition, one can finally rewrite the GME under the form of a purely classical rate equation [as given by Eq. (13)] that governs the kinetic of the excitonic site populations.

By applying this scheme to the extended star and the asymmetric chain, one shows that the two networks transform into two pretty similar “directed chains” as illustrated in Fig. 6. These directed chains include three types of rates noted k_A , k_B , and k_C (plus the irreversible trapping Γ) that read

$$k_A = \frac{2J^2\gamma}{\gamma^2 + \Delta^2}, \quad k_B = \frac{2J^2}{\gamma}, \quad k_C = \frac{2J^2}{\gamma + \Gamma/2}. \quad (14)$$

Note that the form of these rates (obtained from the scheme introduced in Ref. [63]) are similar to the ones present in other works focusing on excitonic diffusion (see for example Refs. [64–66] and references therein). As illustrated in Fig. 6,

the transformation of the asymmetric chain into a directed chain is straightforward. However, this is not the case for the extended star, for which two steps are required. First, the extended star is transformed into a *directed star* (as shown on the right part of Fig. 6) following the steps described previously. Then, starting from the associated rate equation, one introduces a change of variable to replace the total population of each set of symmetrical sites of the directed star (following the circular symmetry of the network) by a single effective population. The resulting $L + 1$ effective populations will be associated with the effective sites of the *directed chain* shown at top right of Fig. 6. Using this mapping, one can show that the resulting directed chain exhibits a very special feature: an anisotropy in the rates linking its two rightmost effective sites (see in Fig. 6). The excitonic transfer towards the trapping core is governed by a rate k_C which is N times lower than the rate Nk_C governing the transfer in the opposite direction. Comparatively, note that the directed network obtained for the asymmetric chain does not present such an asymmetry (here both rates are k_CN as shown in Fig. 6). This exotic phenomenon of anisotropic rate has already been highlighted in numerous studies of dendritic architectures (see Refs. [45,67]). It is directly associated with the connectivity of the central core site, which exhibits a notably higher number of connections (N) than sites located along the branches of the directed star structure.

B. Evolution of the absorption process in the presence of dephasing

Starting from this mapping on directed chains, one can then derive an analytical form for the absorption time. This is indeed possible in the case of directed chains, using approaches based either on the analytical properties of the inverted rate matrix \mathbf{K}^{-1} , or on waiting time distribution formalism (see Refs. [63,68–70] and references therein). We refer interested readers to Appendices C and D, where we provide more details on these two methods. Based on this, one can obtain an analytical form of the excitonic absorption time for both directed chains that reads $\tau \approx \ln(2)\bar{\tau}$, with

$$\bar{\tau} = \frac{\mathcal{N}_S}{\Gamma} + \frac{1}{k_A} + \frac{(L+1)(L-2)}{2k_B} + \frac{L}{k_C} \left(1 + \frac{1-N}{N} \delta^{\text{Ch}} \right). \quad (15)$$

Here k_A , k_B , and k_C are the rates defined in Eq. (14), and δ^{Ch} is a term equal to one only for the asymmetric chain (zero otherwise). Note that the first term \mathcal{N}_S/Γ depends on the total size \mathcal{N}_S of the given network ($\mathcal{N}_S = 1 + L$ for the asymmetric chain, and $\mathcal{N}_S = 1 + NL$ for the extended star). In the following, we will use the analytical form Eq. 15 to interpret the absorption time evolution with dephasing. To this end, we illustrate in Fig. 7 the numerical and analytical results of the variations of τ as a function of γ . The white, gray, and dark gray areas are used to delimit weak, moderate, and strong dephasing regimes respectively. Solid red lines with circles show the analytical results Eq. (15), while solid black curves are for pure numerical simulation. Left and right columns show results for the extended star and the asymmetric chain respectively. Top and bottom rows show

results for two energy defects amplitudes with $\Delta = 0$ (top), and $\Delta = \sqrt{N-1}J$ (bottom). As a reference, we also report on this plot the absorption time obtained without dephasing (horizontal black dotted lines).

To begin, let us focus on the weak dephasing regime $\gamma < 0.1J$ (white area in Fig. 7). As readily seen in the plot, the analytical results fail here to reproduce the numerical simulations. This discrepancy is in fact expected, as in this regime the dephasing is not dominant: Excitonic transport is still strongly coherent (Sec. IV A). With the survival of coherent excitonic transport, it is therefore natural to expect the survival of optimal energy transfer. This is in line with what has been observed in our numerical study (see Sec. III B) regarding the survival of the absorption optimization law in both networks for $\gamma < 0.1J$. Interestingly, even if the excitonic dynamics is still fundamentally coherent in this regime, the presence of dephasing will nevertheless affect the timescale of the absorption process. Indeed, we see in Fig. 7 that an increase in γ causes the absorption time τ (solid black curve) to deviate progressively from the reference time obtained without dephasing (dotted black line). Here the amplitude of τ gradually converges to a plateau that is typically reached when the dephasing enters the moderate dephasing regime $\gamma \rightarrow 0.1J$ (see horizontal dashed red lines in all panels).

The regime of moderate dephasing $\gamma \in [0.1J, 10J]$ (central gray region in Fig. 7) is precisely where a turning point occurs in the nature of excitonic dynamics. In this case, the dephasing amplitude γ becomes comparable to the hopping constant J , so that the diffusive transport point of view begins to be valid (see Sec. IV A). This can be clearly observed in Fig. 7, as the analytical results here start to match the numerical simulations very well. This holds whatever the network and the Δ value considered. Interestingly, in this regime, the absorption time systematically converges towards a plateau value. The latter depends on the network but remains the same whatever Δ (see rows in the same column in Fig. 7). This behavior is consistent with what was highlighted earlier in the Δ -parameter space in Sec. III B 2 (see Fig. 4). Based on the good correspondence between the analytical and numerical behaviors here, one can actually relate the amplitude of this plateau to the first term of Eq. (15), that is, $\tau = \ln(2)\mathcal{N}_S/\Gamma$ (which represents an approximate low bound of the equation). With this analytical form, one can better understand the features evidenced in our numerical study when $\gamma \sim J$. First, the \mathcal{N}_S dependence of the plateau explains why we observe a different timescale in the absorption process occurring on the two networks when the dephasing increases. Indeed, the total number of sites for the extended star $\mathcal{N}_S = 1 + LN$ is larger than for the asymmetric chain $\mathcal{N}_S = 1 + L$. The resulting plateau is thus higher in the first case than in the second. As a consequence, the closer we get to the moderate dephasing regime, the slower the absorption process will be for the star compared to the asymmetric chain. This is in line with what has been observed in our numerical study (see Figs. 3 and 4). Second, it is interesting to note that the plateau value $\tau = \ln(2)\mathcal{N}_S/\Gamma$ is Δ independent. As a result, we understand here that the absorption time will always converge in the moderate dephasing regime to the same plateau whatever Δ (as shown in Fig. 7). This property explains why previously in Fig. 4 (Sec. III B 2) we observed a global flattening of

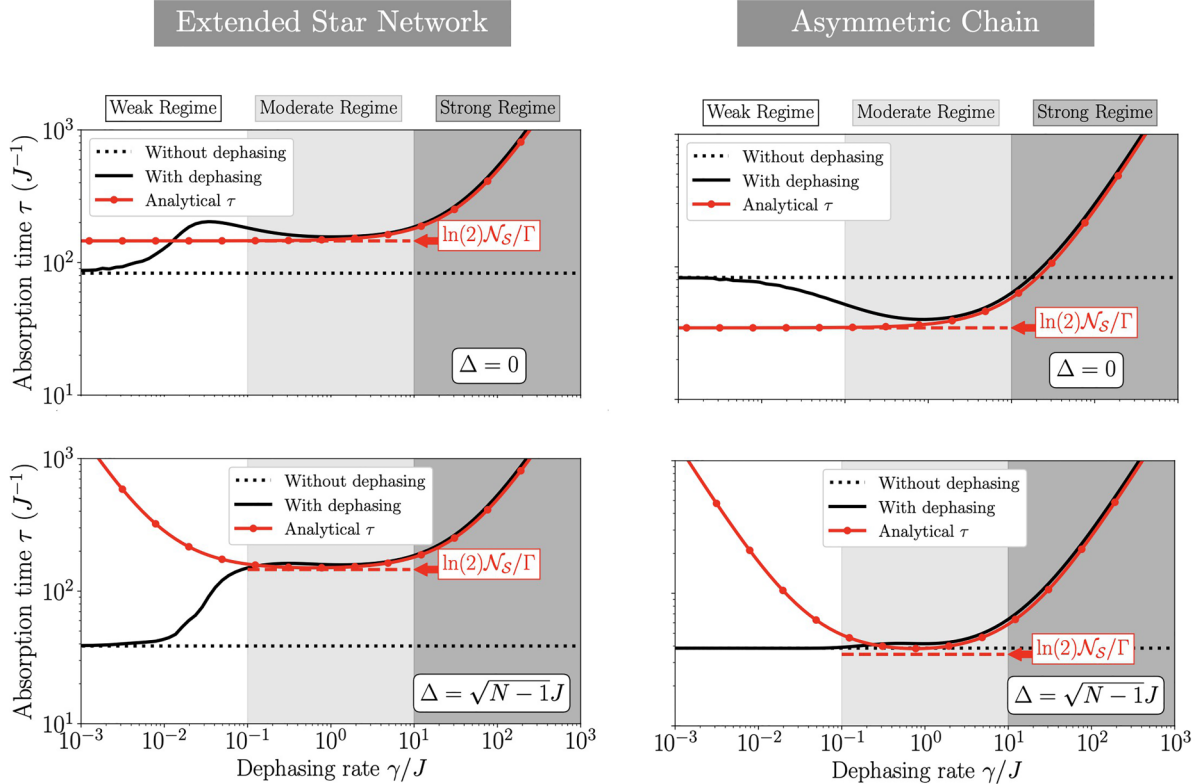


FIG. 7. Evolution of the absorption time τ with the dephasing rate γ for different values of energy defects amplitudes Δ parameters (with $N = 5, L = 4$). Left column: Extended star network. Right column: Asymmetric chain. The results on the top row are for a configuration $\Delta = 0$, whereas the bottom row shows results for $\Delta = \sqrt{N-1}J$. Full and dotted black curves respectively show results with and without dephasing. Red curves with circles show the results of the analytical behavior as given in Eq. (15). Horizontal red dashed lines show the amplitude $\ln(2)\mathcal{N}_S/\Gamma$. In each panel, white, gray, and dark gray areas are used to delimit weak, moderate, and strong dephasing regimes respectively.

the absorption time curves in the Δ -parameters space when $\gamma \rightarrow 0.5J$.

Finally, when the strong dephasing regime is reached (dark gray area in Fig. 7), a second turning point occurs for the excitonic dynamics. In this case, the dephasing is so strong that the excitonic transfer gets hindered, leading to the slowdown of the energy absorption process. This can be readily seen in Fig. 7 with the increase of the absorption time τ with the dephasing amplitude γ . Here again, note the excellent correspondence between the analytical results and the numerical simulations. Based on this, one can understand that the behavior of the absorption time is actually described by the three additional contributions of Eq. (15) that depend on the rates k_A, k_B , and k_C [as defined in Eq. (14)]. Globally, these contributions reveal that the absorption time τ scales (approximately) linearly with the dephasing amplitude, i.e., $\tau \propto \gamma$ when $\gamma \gg J$. Note the presence of a difference in the last term of Eq. (15) which yields L/k_C for the star, and $L/(Nk_C)$ for the asymmetric chain. This reveals that, in the case of the asymmetric chain, the absorption time increases less rapidly with γ than for the star. This feature can directly be related to the anisotropic rates present in the directed chain associated to the extended star (see Fig. 6). In this case, the excitonic energy transfer is biased: The transfer with the rate k_C towards the trap is N times weaker than in the opposite direction where the rate is Nk_C . To conclude our discussion, one should mention

that the arising of the general exciton transfer slowdown in the strong dephasing regime may be in fact linked to the arising of the “quantum Zeno effect” [71] (also known as the “watch-dog effect”). This effect has been extensively discussed in studies focusing on excitonic quantum transport (see for example Refs. [61,72,73]) as an explanation for the limited motion of excitons under extremely strong dephasing conditions. In such scenarios, the exciton’s environment acts akin to an observer, engaging in rapid and frequent measurement-like interactions. These interactions obstruct the coherent spread of the exciton, preventing its delocalization and compelling it to stay localized at its initial site. As a result, this leads to a substantial slowdown in the transfer to the trap, leading to a significant increase in absorption time.

V. CONCLUSION

In this work, we studied the open quantum system dynamics of an exciton and its absorption on two networks: an extended star and an asymmetric chain. The specificity of these two networks was recently highlighted in Ref. [47] where we showed that both architectures actually present a similar energy absorption process that can be optimized by the inclusion of tunable energy defects (in the absence of environment). As a direct extension to this work, our investigations here focused on the question of how this absorption

optimization is affected by the presence of a dephasing, and whether, in practice, the two networks respond differently to the presence of an environment.

Our work revealed that both networks actually present very similar behaviors concerning the survival of the optimization law when the dephasing is increased. In both cases, the absorption process can still be optimized by the use of energy defects as long as the dephasing remains weak enough. In this regime, the only difference between the two networks is the appearance of an offset in the absorption time, which is more significant in the case of the extended star than in the asymmetric chain. Analytical developments based on the diffusive limit of the excitonic transport allowed to connect this behavior to the size of the networks (i.e., the number of sites \mathcal{N}_S). Additionally, our results have shown that for both networks the optimization law is totally lost as soon as we enter moderate and strong dephasing regimes. In this case, analytical developments revealed that the absorption time increases linearly with the dephasing amplitude. This feature can be interpreted as the arising of the so-called quantum Zeno effect.

Therefore, our work evidenced the possibility for both networks to exhibit an absorption optimization mediated by energy defects in the presence of an environment (to some limit). These results naturally motivate new questions that could represent interesting starting points for future developments. For example, it would be interesting to see if the similarities shared by the two networks would resist to the presence of a static disorder (e.g., site energies and/or hopping constants modulations). In this context, the symmetry breaking induced by disorder should open new paths on the networks for the excitonic dynamics leading to potential different absorption mechanisms. Moreover, we could also consider exploring different types of architecture (e.g., dendrimers, Cayley trees and other hyperbranched networks). Finally, it would be also interesting to see if more realistic excitonic environment modeling would lead to new behaviors (e.g., full quantum description of the phonons). Indeed, in the current work we employed a Lindblad master equation (i.e., HSR model) which is fundamentally Markovian and thus excludes the possibility of observing long-term quantum coherence in the system. This description prevents us from observing any potential exotic non-Markovian effects that would naturally arise in the excitonic transport. All these ideas will be considered in future projects and papers.

APPENDIX A: SIMILARITY IN THE EXCITONIC TRANSPORT ON THE EXTENDED STAR NETWORK AND THE ASYMMETRIC CHAIN

Let us consider the extended star graph with N branches of length L on which the exciton dynamics is governed by the Hamiltonian H Eq. (1). H being invariant under the discrete rotation of angle $\theta = 2\pi/N$ and centered on the core of the star, its diagonalization is simplified when one works with an intermediate basis involving the state localized on the core $|0, 0\rangle$ and a set of orthogonal Bloch states $|\chi_s^{(k)}\rangle$ with $s = 1, 2, \dots, L$ and $k = 1, 2, \dots, N$. A given Bloch state is

defined as

$$|\chi_s^{(k)}\rangle = \frac{1}{\sqrt{N}} \sum_{b=1}^N e^{-ikb\theta} |b, s\rangle. \quad (\text{A1})$$

Within this basis, H is expressed as a direct sum $H = H^{(1)} \oplus H^{(2)} \dots \oplus H^{(N)}$, where $H^{(k)}$ is the block Hamiltonian associated to the good quantum number k . For all $k \neq N$, all the block $H^{(k)}$ are identical. They are expressed as

$$H^{(k \neq N)} = \sum_{s=1}^L (\epsilon_0 + \Delta\delta_{sL}) |\chi_s^{(k)}\rangle \langle \chi_s^{(k)}| + \sum_{s=1}^{L-1} J (|\chi_{s+1}^{(k)}\rangle \langle \chi_s^{(k)}| + |\chi_s^{(k)}\rangle \langle \chi_{s+1}^{(k)}|). \quad (\text{A2})$$

For $k = N$, the Hamiltonian $H^{(N)}$ is defined as

$$H^{(N)} = \left(\epsilon_0 - i\frac{\Gamma}{2} \right) |0, 0\rangle \langle 0, 0| + \sum_{s=1}^L (\epsilon_0 + \Delta\delta_{sL}) |\chi_s^{(N)}\rangle \langle \chi_s^{(N)}| + \sqrt{N} J (|0, 0\rangle \langle \chi_1^{(N)}| + |\chi_1^{(N)}\rangle \langle 00|) + \sum_{s=1}^{L-1} J (|\chi_{s+1}^{(N)}\rangle \langle \chi_s^{(N)}| + |\chi_s^{(N)}\rangle \langle \chi_{s+1}^{(N)}|). \quad (\text{A3})$$

One sees here that when the exciton is initially uniformly delocalized over the peripheral sites of the star (i.e., with an initial state $|\chi_s^{(N)}\rangle$), its dynamics is confined in the $k = N$ subspace. Restricting our attention to that subspace, the notations can be simplified by renaming the basis vectors as

$$|s\rangle = \begin{cases} |0, 0\rangle & \text{if } s = 0 \\ |\chi_s^{(N)}\rangle & \text{if } s > 0 \end{cases}. \quad (\text{A4})$$

Within these notations, the restriction of the Hamiltonian in the $k = N$ subspace is rewritten as

$$H^{(N)} = \sum_{s=0}^L \left(\epsilon_0 - i\frac{\Gamma}{2} \delta_{s0} + \Delta\delta_{sL} \right) |s\rangle \langle s| + \sum_{s=1}^{L-1} J (|s\rangle \langle s+1| + |s+1\rangle \langle s|) + J\sqrt{N} (|0\rangle \langle 1| + |1\rangle \langle 0|). \quad (\text{A5})$$

Equation (A5) corresponds to the Hamiltonian given in Eq. (2) which governs the exciton dynamics on the asymmetric chain shown in Fig. 1.

APPENDIX B: REDUCED SET OF EQUATIONS FOR THE EXCITONIC DYNAMICS ON THE EXTENDED STAR NETWORK

Studying the absorption process on the extended star needs the knowledge of the time evolution of the absorption probability $P_A(t)$ [Eq. (7)]. Because, it depends only on the trace of the exciton RDM $\rho(t)$, its characterization does not require to resolve the full set of \mathcal{N}_S^2 coupled equations describing

the dynamics of the GME Eq. (3) (which numerically scales in \mathcal{N}_S^6 for the FLS method). Instead, one can only focus on a reduced number of quantities thus reducing drastically the numerical cost needs to solve the problem.

To proceed, let us define the four key quantities we should focus on: First, the core population,

$$P_0 = \rho_{00,00}; \quad (\text{B1})$$

second, the peripheral intrabranches populations and coherences,

$$P_{ss'} = \sum_{b=1}^N \rho_{bs,bs'}, \quad (\text{B2})$$

which represent a $(L \times L)$ matrix whose elements are independent on the number of branches and depend only on the size of the branches. The diagonal elements contain the populations of each generation of the graph while the nondiagonal elements characterize the coherences between sites of the

same branch. Third, we have the interbranches coherences,

$$C_{ss'} = \sum_{b=1}^N \sum_{b'=1}^N (1 - \delta_{bb'}) \rho_{bs,b's'}, \quad (\text{B3})$$

which represent a $(L \times L)$ matrix whose elements characterize the coherences between different branches only. And finally, there are the core-branch coherences,

$$K_s = \sum_{b=1}^N \rho_{bs,00}, \quad (\text{B4})$$

which represents a column vector of dimension L whose elements characterize the coherences between the core and the branch sites.

Using these key quantities, the excitonic dynamics is governed by a reduced set of $n_S = 1 + 2L + 2L^2$ coupled equations reading

$$\begin{aligned} \partial_t P_0 &= -\Gamma P_0 - iJ(K_1 - K_1^*) \\ \partial_t P_{ss'} &= -i \sum_{s''} (h_{ss''} P_{s''s'} - P_{ss''} h_{s''s'}) + iJ(K_s \delta_{s',1} - K_s^* \delta_{s,1}) - \gamma P_{ss'} (1 - \delta_{ss'}) \\ \partial_t C_{ss'} &= -i \sum_{s''} (h_{ss''} C_{s''s'} - C_{ss''} h_{s''s'}) + iJ(N-1)(K_s \delta_{s',1} - K_s^* \delta_{s,1}) - \gamma C_{ss'} \\ \partial_t K_s &= -\left(\frac{\Gamma}{2} + \gamma\right) K_s - i \sum_{s''} h_{ss''} K_{s''} + iJ(P_{s1} + C_{s1}) - iJNP_0 \delta_{s1} \\ \partial_t K_s^* &= -\left(\frac{\Gamma}{2} + \gamma\right) K_s^* + i \sum_{s''} h_{ss''} K_{s''}^* - iJ(P_{1s} + C_{1s}) + iJNP_0 \delta_{s1}, \end{aligned} \quad (\text{B5})$$

where \mathbf{h} represents a $(L \times L)$ reduced Hamiltonian matrix defined as

$$\mathbf{h} = \begin{pmatrix} 0 & J & & & & \\ J & 0 & J & & & \\ & J & \dots & & & \\ & & & 0 & J & \\ & & & J & \Delta & \end{pmatrix}. \quad (\text{B6})$$

The reduced set of differential equations Eq. (B5) can be put into a compact matrix form

$$\partial_t \mathbf{v} = \mathbf{G} \mathbf{v}, \quad (\text{B7})$$

where \mathbf{v} is a column vector (dimension n_S) containing all the elements of the key quantities introduced before (the matrices have been flattened), and \mathbf{G} is the square generatrix matrix encoding the coefficients of the differential equations (with dimension n_S^2). A left or right eigendecomposition can be conducted on \mathbf{G} to exponentiate the associated matrix and consequently to solve the time evolution of the key quantities as

$$\mathbf{v}(t) = \exp(\mathbf{G}t) \mathbf{v}(0). \quad (\text{B8})$$

With this approach, the absorbed population at time t is obtained by summing the pertinent elements of the vector \mathbf{v}

returning

$$P_A(t) = 1 - P_0(t) - \sum_s P_{ss}(t). \quad (\text{B9})$$

Note that the numerical cost of the FLS method based on this reduced set of equations will scale in n_S^3 , which is drastically lower compared to the original cost in \mathcal{N}_S^6 (i.e., exact diagonalization of a matrix with dimension n_S instead of \mathcal{N}_S^2).

APPENDIX C: ANALYTICAL FORM OF THE EXCITONIC ABSORPTION TIME ON A DIRECTED LINEAR NETWORK USING THE PROPERTIES OF THE INVERSE RATE MATRIX

When considering an intermediate or strong dephasing ($\gamma \geq J$), the excitonic dynamics on both networks reduces to a random walk on a directed chain with a trap, as depicted in Fig. 8. Starting from this view, we will detail in this Appendix how to estimate the excitonic absorption time using the concept of ‘‘mean first passage time’’ (MFPT) [74].

The MFPT, noted $\bar{\tau}$, defines the typical time for a random walker starting from an initial node of a given directed graph to reach another specific distant targeted node. If the target node contains a trap, then $\bar{\tau}$ can be seen as the typical time required for the random walker to initiate its irreversible

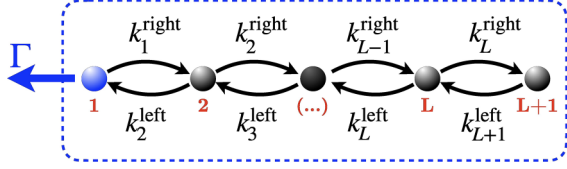


FIG. 8. Directed chain of length $\mathcal{N}_S = L + 1$ with an irreversible trapping process occurring on the first site with a rate Γ .

trapping process. In our study, we will focus on the case of a random walker evolving on the directed chain of length $L + 1$ as shown in Fig. 8. We will assume here that the initial node occupied by the walker is on the right extremity of the chain (site $L + 1$). The targeted node will be the one at the other extremity of the chain (site 1) where an irreversible trapping process takes place (with rate Γ). On this chain, the walker hops between nodes with left or right oriented rate constants noted $k_s^{\text{left}}/k_s^{\text{right}}$ with “ s ” the index of the site from which the hops come from. All this information is collected in a rate matrix \mathbf{K} that reads

$$\mathbf{K} = \begin{bmatrix} -\Gamma - k_1^{\text{right}} & k_2^{\text{left}} & & & & \\ k_1^{\text{right}} & -k_2^{\text{right}} - k_2^{\text{left}} & k_3^{\text{left}} & & & \\ & k_2^{\text{right}} & \dots & \dots & & \\ & & \dots & \dots & k_{L+1}^{\text{left}} & \\ & & & & k_L^{\text{right}} & -k_{L+1}^{\text{left}} \end{bmatrix}. \quad (\text{C1})$$

From the knowledge of \mathbf{K} , the time evolution of the random walker is formally given by

$$\mathbf{P}(t) = \exp(\mathbf{K}t)\mathbf{P}(0), \quad (\text{C2})$$

where $\mathbf{P}(0) = (P_1(0), P_2(0), \dots, P_{L+1}(0))^T$ is a column vector that encodes the initial sites populations (walker starting on site $L + 1$) and $\mathbf{P}(t)$ the resulting time-evolved vector at time t . Within these notations, the MFPT is defined as

$$\bar{\tau} = \sum_{s=1}^{L+1} \int_0^{+\infty} P_s(t) dt. \quad (\text{C3})$$

Formally, this quantity can be seen as the sum of the residence time of the walker on all the sites (see Ref. [74]), which provides an estimate of how long the walker “survives” on the network before starting to feel the effect of the trap on site 1. Due to the irreversible trapping, we know that for $t \rightarrow +\infty$ we have $\exp(Kt) \rightarrow 0$. Using this property, one can integrate Eq. (C3) and shows that the MFPT takes the following form:

$$\bar{\tau} = - \sum_{s=1}^{L+1} [\mathbf{K}^{-1}\mathbf{P}(0)]_s. \quad (\text{C4})$$

As shown here, the elements of the inverse rate matrix \mathbf{K}^{-1} provide an estimate of the MFPT. In practice, getting access to the analytical form of \mathbf{K}^{-1} is a very difficult task. However, it has been shown (see Ref. [68]) that this information can be exactly accessed in the case of directed chains *via* recurrence

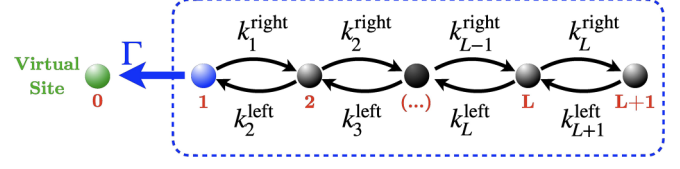


FIG. 9. Directed chain of length $\mathcal{N}_S = L + 2$ with an irreversible trapping process occurring between sites $1 \rightarrow 0$ with a rate Γ .

relations. In this case, the exact form of \mathbf{K}^{-1} allows us to derive an analytical form of the MFPT that reads (see Eq. (19) in Ref. [68])

$$\bar{\tau} = \sum_{m=1}^{L+1} r_m + \sum_{m=1}^L \frac{1}{r_m k_m^{\text{right}}} \sum_{n=m+1}^{L+1} r_n, \quad (\text{C5})$$

with the amplitudes r_m defined as

$$r_m = \begin{cases} \frac{1}{\Gamma}, & \text{for } m = 1. \\ \frac{1}{\Gamma} \frac{k_1^{\text{right}} k_2^{\text{right}} \dots k_{m-1}^{\text{right}}}{k_2^{\text{left}} k_3^{\text{left}} \dots k_m^{\text{left}}}, & \text{for } m > 1. \end{cases} \quad (\text{C6})$$

We can determine the shape of these amplitudes for the two directed chains associated to the extended star network and the asymmetric chain. In the case of the extended star we have

$$r_m = \begin{cases} 1/\Gamma, & \text{for } m = 1. \\ N/\Gamma, & \text{for } m > 1. \end{cases} \quad (\text{C7})$$

While for the case of the asymmetric chain we have

$$r_m = \frac{1}{\Gamma}, \quad \text{for } m \geq 1. \quad (\text{C8})$$

By injecting these amplitudes in Eq. (C5), one can finally derive the analytical form of the MFPT $\bar{\tau}$ given in Eq. (15) for both networks.

APPENDIX D: ANALYTICAL FORM OF THE EXCITONIC ABSORPTION TIME ON DIRECTED LINEAR NETWORKS USING THE WAITING TIME DISTRIBUTION FORMALISM

In complement to Appendix C, let us describe an alternative approach to determine the absorption time in the strong dephasing limit. This approach is based on the “*waiting time distribution*” formalism (see Ref. [69]), which is a mathematical tool that has been used in various fields ranging from excitonic transport [63] to single-molecule chemical chain reactions [69,75–78].

As depicted in Fig. 9, the linear chain considered here now extends to a length of $L + 2$ (and not $L + 1$, as in Appendix 9 and throughout the paper). This extension includes an additional “virtual” site (highlighted in green in Fig. 9), responsible for irreversible absorption of excitonic population at a rate Γ . This alteration transforms the system behavior away from strict dissipativity: The chain is now “closed” and the excitonic population is irreversibly stored within the virtual site with a rate Γ . Importantly, this adjustment does not compromise the core problem under investigation but serves as a crucial element supporting the mathematical developments outlined in this Appendix.

- [31] K. Harigaya, *Chem. Phys. Lett.* **300**, 33 (1999).
- [32] E. Y. Poliakov, V. Chernyak, S. Tretiak, and S. Mukamel, *J. Chem. Phys.* **110**, 8161 (1999).
- [33] T. Minami, S. Tretiak, V. Chernyak, and S. Mukamel, *J. Lumin.* **87–89**, 115 (2000).
- [34] M. Nakano, M. Takahata, H. Fujita, S. Kiribayashi, and K. Yamaguchi, *Chem. Phys. Lett.* **323**, 249 (2000).
- [35] J. C. Kirkwood, C. Scheurer, V. Chernyak, and S. Mukamel, *J. Chem. Phys.* **114**, 2419 (2001).
- [36] M. A. Martín-Delgado, J. Rodríguez-Laguna, and G. Sierra, *Phys. Rev. B* **65**, 155116 (2002).
- [37] M. Nakano, M. Takahata, S. Yamada, K. Yamaguchi, R. Kishi, and T. Nitta, *J. Chem. Phys.* **120**, 2359 (2004).
- [38] C. Supritz, A. Engelmann, and P. Reineker, *J. Lumin.* **111**, 367 (2005).
- [39] G. W. Crabtree and N. S. Lewis, *Phys. Today* **60**(3), 37 (2007).
- [40] M. Nakano, R. Kishi, T. Minami, and K. Yoneeda, *Molecules* **14**, 3700 (2009).
- [41] V. Pouthier, *Phys. Rev. E* **90**, 022818 (2014).
- [42] A. W. Bosman, H. M. Janssen, and E. W. Meijer, *Chem. Rev.* **99**, 1665 (1999).
- [43] F. Vogtle, G. Richardt, and N. Werner, *Dendrimer Chemistry: Concepts, Syntheses, Properties, Applications* (Wiley, Weinheim, 2009).
- [44] D. Astruc, E. Boisselier, and C. Ornelas, *Chem. Rev.* **110**, 1857 (2010).
- [45] A. Bar-Haim, J. Klafter, and R. Kopelman, *J. Am. Chem. Soc.* **119**, 6197 (1997).
- [46] M. S. Choi, T. Aida, T. Yamazaki, and I. Yamazaki, *Chem. Eur. J.* **8**, 2667 (2002).
- [47] S. Yalouz and V. Pouthier, *Phys. Rev. E* **106**, 064313 (2022).
- [48] E. Joos, H. D. Zeh, C. Kiefer, D. Giulini, J. Kupsch, and I. O. Stamatescu, *Decoherence and the Appearance of a Classical World in Quantum Theory* (Springer, New York, 2003).
- [49] M. Schlosshauer, *Decoherence and the Quantum-to-Classical Transition* (Springer Verlag, Berlin, 2007).
- [50] P. Breuer and F. Petruccione, *The Theory of Open Quantum Systems* (Oxford University Press, New York, 2007).
- [51] V. Pouthier, *Phys. Rev. E* **78**, 061909 (2008).
- [52] V. Pouthier, *Phys. Rev. B* **80**, 144304 (2009).
- [53] H. Haken and P. Reineker, *Z. Phys.* **249**, 253 (1972).
- [54] H. Haken and G. Strobl, *Z. Phys.* **262**, 135 (1973).
- [55] B. Jackson and R. Silbey, *J. Chem. Phys.* **75**, 3293 (1981).
- [56] I. Rips, *Phys. Rev. E* **47**, 67 (1993).
- [57] W. Pfluegl, M. A. Palenberg, and R. Silbey, *J. Chem. Phys.* **113**, 5632 (2000).
- [58] V. V. Sokolov and V. G. Zelevinsky, *Nucl. Phys. A* **504**, 562 (1989).
- [59] V. V. Sokolov and V. G. Zelevinsky, *Ann. Phys.* **216**, 323 (1992).
- [60] M. B. Plenio and S. F. Huelga, *New J. Phys.* **10**, 113019 (2008).
- [61] P. Rebentrost, M. Mohseni, I. Kassal, S. Lloyd, and A. Aspuru-Guzik, *New J. Phys.* **11**, 033003 (2009).
- [62] P. Virtanen *et al.*, *Nat. Methods* **17**, 261 (2020).
- [63] J. Cao and R. J. Silbey, *J. Phys. Chem. A* **113**, 13825 (2009).
- [64] Y. Zhang, G. L. Celardo, F. Borgonovi, and L. Kaplan, *Phys. Rev. E* **95**, 022122 (2017).
- [65] Y. Zhang, G. L. Celardo, F. Borgonovi, and L. Kaplan, *Phys. Rev. E* **96**, 052103 (2017).
- [66] J. A. Leegwater, *J. Phys. Chem.* **100**, 14403 (1996).
- [67] C. Monthus and C. Texier, *J. Phys. A: Math. Gen.* **29**, 2399 (1996).
- [68] A. Bar-Haim and J. Klafter, *J. Chem. Phys.* **109**, 5187 (1998).
- [69] J. Cao and R. J. Silbey, *J. Phys. Chem. B* **112**, 41 (2008).
- [70] I. V. Gopich and A. Szabo, *J. Chem. Phys.* **118**, 454 (2003).
- [71] B. Misra and E. C. G. Sudarshan, *J. Math. Phys.* **18**, 756 (1977).
- [72] L. Novo, M. Mohseni, and Y. Omar, *Sci. Rep.* **6**, 18142 (2016).
- [73] S. Pouyandeh, S. Iubini, S. Jurinovich, Y. Omar, B. Mennucci, and F. Piazza, *Phys. Biol.* **14**, 066001 (2017).
- [74] N. F. Polizzi, M. J. Therien, and D. N. Beratan, *Isr. J. Chem.* **56**, 816 (2016).
- [75] I. V. Gopich and A. Szabo, *J. Chem. Phys.* **124**, 154712 (2006).
- [76] A. Kolomeisky and M. F. Fisher, *J. Chem. Phys.* **113**, 10867 (2000).
- [77] D. Singh, B. Punia, and S. Chaudhury, *ACS Omega* **7**, 47587 (2022).
- [78] S. C. Kou, B. J. Cherayil, W. Min, B. P. English, and S. X. Xie, *J. Phys. Chem. B* **109**, 19068 (2005).